THE ASTRONOMICAL JOURNAL VOLUME 88, NUMBER 4 APRIL 1983

RADAR OBSERVATIONS OF ASTEROID 1685 TORO

STEVEN J. OSTRO
Department of Astronomy, Cornell University, Ithaca, New York 14853

DONALD B. CAMPBELL
National Astronomy and Ionosphere Center,[a] Arecibo, Puerto Rico 00613

IRWIN I. SHAPIRO
Harvard-Smithsonian Center for Astrophysics, Cambridge, Massachusetts 02138
Received 9 November 1982; revised 22 December 1982

ABSTRACT

We report results of 13-cm-wavelength radar observations of 1685 Toro conducted in July 1980 at the Arecibo Observatory. Our data yield detections of radar echoes in the same sense of circular polarization as transmitted (i.e., the SC sense) as well as in the opposite (OC) sense. The radar spectra reveal correlated, approximately twofold variations in radar cross section and spectral bandwidth as functions of rotational phase, with two maxima and two minima per rotation cycle. Our estimate of the ratio of SC to OC echo power, $\mu_c = 0.18 \pm 0.04$, suggests that most, but certainly not all, of the backscattering is due to single reflections from surface elements that are fairly smooth at decimeter scales. However, the total absence of the sharply peaked spectral signature of quasi-specular scattering requires substantial roughness at some much larger scale(s). When combined with photopolarimetric results of Dunlap *et al.* (1973), our observations provide constraints on Toro's size, shape, and surface properties. The maximum distance of any part of Toro's surface from the spin axis is between 2.4 and 3.4 km. The ratio of Toro's longest to shortest equatorial widths is between 1.4 and 2.2. Modeling Toro as a homogeneously scattering ellipsoid yields weighted-least-squares estimates for the lengths of the equatorial semiaxes: $a = 2.60 \pm 0.10$ km and $b = 1.68 \pm 0.17$ km, and a nearly Lambertian scattering law. The magnitude of the post-fit residuals suggests systematic departures of Toro from this simplified model, including a possible surface feature with enhanced radar reflectivity and depolarization. The length, $2c$, of the rotation axis cannot be estimated from our data, as it is highly anticorrelated with the radar reflectivity. If we assume that $c \leqslant b$, our ellipsoid provides $\pi ab = 13.7 \pm 1.8$ km^2 as an estimate for an upper limit on Toro's projected area. Using this result, we derive approximate lower limits on Toro's λ 13-cm and B-filter geometric albedoes (0.04 and 0.23, respectively) which constrain the composition and porosity of Toro's surface. Our lower bound on Toro's B-filter albedo is substantially higher than the value (0.14) reported by Dunlap *et al.*

I. INTRODUCTION

The minor planet 1685 Toro is one of the more thoroughly studied Earth-crossing Apollo asteroids. The widely recognized scientific importance of planet-crossing objects (including Atens, Apollos, and Amors) stems from their possible genetic relationships to meteorites, comets, and mainbelt asteroids, and from their apparently dominant role in the collisional history of the inner solar system. Although Toro may eventually suffer the same violent demise presumed for other Apollos, it is protected from close planetary encounters during at least the next $\sim 10^6$ yr by an unusual resonance which involves alternation between orbital librations in a 5/8 commensurability with Earth and a 5/13 commensurability with Venus (Greenberg and Scholl 1979; Williams and Wetherill 1973).

Our knowledge of the physical properties of small planetary objects is embarrassingly sparse. Apollo asteroids remain below the current sensitivity thresholds of the more sophisticated VIS/IR ground-based astronomical techniques except during their closest approaches to Earth. In the case of Toro, its unique resonance currently provides favorable observation opportunities (Earth-Toro distance < 0.2 AU) at eight-year intervals. During its 1972 apparition, Toro was studied with photopolarimetry (Dunlap, Gehrels, and Howes 1973), spectrophotometry (Chapman, McCord,

[a] Operated by Cornell University under contract with the National Science Foundation and with support from the National Aeronautics and Space Administration.

and Pieters 1973; Johnson and Matson 1973), and radar (Goldstein, Holdridge, and Lieske 1973).

Dunlap *et al.* (1973), hereafter referred to as DGH, obtained light curves, *UBV* colors, and rotational polarization curves for solar phase angles (i.e., Sun-Toro-Earth angles) between 32° and 99°. They estimated a polarimetric geometric albedo in the B filter equal to 0.14 ± 0.03, implying a mean value for the effective radius of 2.2 ± 1.5 km when coupled with their other photometric results. [*Note*: All uncertainties in DGH are "probable errors." For a Gaussian error distribution, the probable error is 0.6745 standard deviations (Snedecor and Cochran 1980, p. 43). We have scaled all uncertainties in DGH to their standard-deviation equivalent *prior* to quoting them here.] DGH's light curves provided estimates of Toro's synodic rotation period for various intervals during July–August, 1972, and analyses of these data yielded estimates of the magnitude and direction of Toro's spin vector (sidereal period $= 19.1956 \pm 0.0016$ hr; ecliptic longitude, latitude of pole $= 200° \pm 30°$, $55° \pm 7°$). DGH also deduced that Toro's "shape is elongated, and probably irregular, with a cross-sectional area ratio of about 3.2, the maximum effective radius is 2.8 km and the minimum 1.6 km."

Chapman *et al.* (1973) obtained 18- and 22-filter VIS/IR reflection spectra that display a prominent pyroxene (0.95–1.00 μm) absorption and closely resemble reflection spectra of *L* (4–6) chondritic meteorites. Their work marked the first narrowband spectrophotometry of a non-main-belt asteroid and also provided the first convincing spectral match between a minor planet and ordinary chondrites. Results of the 0.4–0.8 μm spectrophotometry by Johnson and Matson (1973) were compatible with those of Chapman *et al.* (1973).

Goldstein *et al.* (1973) conducted λ 13-cm radar observations of Toro at the Jet Propulsion Laboratory's Goldstone Tracking Station. Their echo power spectrum, obtained by summing five hours of radar data taken over two nights, provided a lower limit, 1.7 km, on Toro's maximum equatorial radius, consistent with the DGH photopolarimetric results.

Prior to these Toro observations, radar echoes from 1566 Icarus had been detected at JPL by Goldstein (1968, 1969) and at the Haystack Observatory by Pettengill *et al.* (1969). However, the information content of these first two applications of radar techniques to minor planets was severely limited by the sensitivity of the available instruments. As useful planetary radars, these systems have now been largely replaced by much more powerful instruments at the Arecibo Observatory (λ 13 cm) and JPL (λ 3.5 cm).

The potential contribution of radar to asteroid science is considerable (Jurgens and Bender 1977; Chapman and Zellner 1978; Morrison and Niehoff 1979) and has been most fully realized in the case of 433 Eros (Jurgens and Goldstein 1976; Campbell *et al.* 1976; see Pettengill and Jurgens 1979, for a review of asteroid radar observations). Resolution of the radar echo in Doppler shift or time delay can provide a high degree of spatial resolution, independent of an asteroid's apparent angular size. Radar can also provide independent constraints on an asteroid's size, shape, spin vector, and, to a much more limited extent, surface composition and density. By virtue of the wavelengths employed, dual-polarization measurements provide information about structural scales ($\sim 10^{-2}$ m to $\sim 10^{2}$ m) intermediate between scales probed by optical polarimetry and the scales of asteroid diameters.

In this paper we report 13-cm-wavelength, dual-circular-polarization radar observations of Toro conducted at the Arecibo Observatory in July 1980, shortly before its closest approach to Earth. In the following section we review the observations and our data-reduction procedures. In Sec. III we describe and interpret physically the characteristics of Toro's radar signature (i.e., reflectivity, polarization, and spectral bandwidth), first in terms of averages over all available rotational phases and then as functions of rotational phase. In Sec. IV we report results of least-squares fits to the radar data of models parameterizing Toro's shape as a triaxial ellipsoid and as a cylinder with hemispherical ends. Throughout, we discuss radar constraints on the size, shape, and surface configuration of Toro in the context of previous VIS/IR/RADAR investigations.

II. OBSERVATIONS AND DATA REDUCTION

We observed Toro on the seven UT dates: 1980 July 19–25, completing an average of seven transmit/receive cycles, or "runs," on each date. Each run consisted of transmission of a highly monochromatic, circularly polarized signal for a duration (~ 200 s) approximately equal to the round-trip propagation time to Toro, followed by reception of the echo for a similar duration. Using an ephemeris generated from prior estimates of Toro's orbital elements, we continually adjusted the receiver frequency to remove the Doppler shift introduced by the changing line-of-sight component of Toro's relative velocity. Received signals were digitized, Fourier transformed by an on-line array processor, and accumulated as real-time power spectra, which were recorded on magnetic tape at convenient intervals. We later processed the data from each run in turn, removing the noise background in the manner described in detail by Ostro *et al.* (1980). Each resultant power spectrum consisted of 365 independent samples at 1.2-Hz intervals.

For each run, reception was in either the *same* rotational sense of *circular* polarization (i.e., the "SC" sense) or the opposite ("OC") sense. Since the handedness of a circularly polarized wave is reversed upon normal reflection from a smooth dielectric interface, the OC sense dominates echoes from planetary surfaces that look smooth at the observing wavelength. (A single dielectric interface with minimum radius of curvature $\gg \lambda$ would "look smooth.") The presence of an SC component can be due either to multiple scattering or to reflections from

TABLE I. Observations.[a]

Date (1980 July)	Number of runs OC	SC	Rotational phase coverage	RA (hr)	DEC (deg)	Ecliptic long. (deg)	lat. (deg)
19	7	7	78°–145°	22.30	16.8	343.1	25.4
20	4	3	227°–274°	22.35	18.4	344.5	26.6
21	8	6	329°–36°	22.39	20.2	345.9	28.0
22	2	0	126°, 160°	22.44	22.1	347.5	29.4
23	13	4	224°–291°	22.50	24.1	349.4	30.9
24	3	0	54°, 58°, 63°	22.61	26.1	352.0	32.1
25	10	6	127°–191°	22.68	28.3	354.1	33.6

[a] Phases correspond to the midpoint of data reception within a run. Phases are calculated with respect to that at 04:00 UT on 1980 July 19, for a constant synodic period of 10.176 hr.

interfaces that are rough at small ($\sim\lambda$) scales. The ratio, μ_c, of SC to OC power is thus a useful indicator of surface/subsurface "roughness." Our nightly pattern of run-to-run polarization selection was designed to provide estimates of Toro's μ_c at diverse rotational phases, Φ.

The week of observations produced a total of 47 OC spectra and 26 SC spectra. Summation of the spectra revealed detections of OC and SC echoes centered several Hz from the expected Doppler frequency and extending over fewer than 13 spectral points, comprising only a few percent of the available bandwidth. For each run, we fit by least squares a straight line to the ~ 350 echo-free points. The resultant lines were characterized by slopes and intercepts close to zero, demonstrating the efficiency of the background-removal procedure applied previously. (The lines' total vertical excursions averaged 0.15 standard deviations of the background noise and never exceeded 0.5 standard deviations.) To ensure the completeness of background removal, we subtracted the contribution of each line from each of the corresponding 365 spectral points.

When normalized to the *a priori* rms fluctuation in the background noise power, the echo-free portions of the background-free spectra were expected to be independent samples of a Gaussian random process with zero mean and unit variance. Chi square goodness-of-fit tests (Snedecor and Cochran, pp. 75–78), performed on each run, confirmed agreement between the *a priori* and *a posteriori* noise statistics.

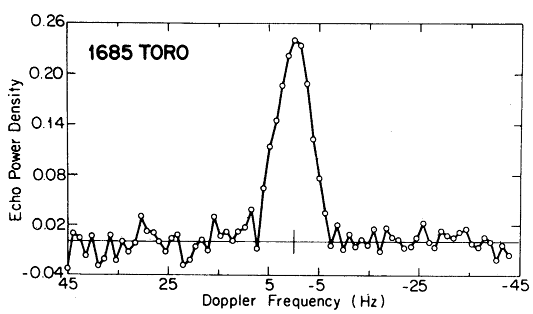

FIG. 1. Toro's radar echo power spectrum in the OC polarization, averaged over all available rotational phases. Echo power density, in units of km^2 of radar cross section per 1.2-Hz resolution cell, is plotted against Doppler frequency. Only the central 20% of the available bandwidth is shown. The central vertical bar represents plus and minus one standard deviation of the background noise.

III. DATA ANALYSIS: TORO'S RADAR SIGNATURE

Table I lists, for each observation date, the OC/SC breakdown of runs, the mean geocentric coordinates of Toro, and the range of rotational phases spanned. Each radar run represents a 200-s integration which spans about 2° of rotational phase. All rotational phases in this paper are relative to that at an arbitrary, but specified, epoch and are based on a value for the synodic period, $P = 10.176$ hr $= 0.4240$ d. This value is a weighted mean of DGH estimates of P derived from light curves obtained for 1972 Toro-Earth configurations similar to those of 1980 July 19–25. Uncertainty in P (due primarily to uncertainty in Toro's spin vector; see below) corresponds to an uncertainty $< 2°$ in our assigned phases.

Figure 1 shows the central 90 Hz of a weighted sum of all OC runs. In this figure, echo power spectral density, in units of km^2 of radar cross section per 1.2-Hz resolution cell, is plotted against Doppler frequency. (Radar cross section equals 4π times the backscattered power per steradian per unit of flux incident at the target.) The central vertical bar on the abscissa represents plus and minus one standard deviation of the receiver noise.

As noted earlier, the central Doppler shift of Toro's radar echo differed from our ephemeris prediction by a few Hz. We estimated the amount of this shift, f_0, by fitting to the data in Fig. 1 a spectral model of the form $S(f) \sim [1 - (f - f_0)^2/(B/2)^2]^{n/2}$, where B is the full bandwidth. This function describes the spectral shape of the radar echo from a spherical target with a homogeneous scattering law, $\sigma_0(\theta) = d\sigma/dA \sim \cos^n \theta$, where σ is radar cross section, dA is a differential element of surface area, and θ is the angle of incidence measured from the normal to dA. However, when applied to objects of unknown shape, $S(f)$ is merely a convenient parameterization of spectral shape, and no specific physical connotation should be attached to n.

Minimizing chi square, (i.e., the weighted sum of the squared residuals) yielded the values: $f_0 = -2.8 \pm 0.2$

Hz, $B = 15.4 \pm 0.9$ Hz, and $n = 3.6 \pm 1.4$. Chi square, calculated for the 13 points closest to the center of the echo spectrum, equals 8.0. Within the quoted standard errors*, the value for f_0 agrees with (i) estimates obtained in a similar manner, but with n fixed successively at integral values between 1 and 10; (ii) the weighted mean of values for f_0 derived from fits of the same "$S(f)$" model to subsets of the 47 individual OC spectra, as discussed below; and (iii) estimates of f_0 based on ellipsoidal models of Toro, discussed in the next section. The estimated value of f_0, which has been subtracted from the abscissa scale in Fig. 1, represents a fractional error of $\sim 2 \times 10^{-5}$ in our observing ephemeris. Correcting our ephemeris accordingly and referring our measurement to an epoch (1980 July 22 at 7^h UTC) near the midpoint of our observations, we obtain an estimate, 161393.5 ± 0.2 Hz, for the Doppler shift at a transmitter frequency of 2380 MHz.

In the following paragraphs we focus on particular aspects of Toro's radar signature (bandwidth, radar cross sections, polarization ratio) and their relation to Toro's physical properties. Although the bandwidth of the weighted mean spectrum (Fig. 1) establishes a constraint on Toro's size, the observed dependence of bandwidth on rotational phase provides the most useful information about Toro's shape. Estimates of Toro's radar cross section and polarization ratio, when coupled with size and shape information, constrain the structural configuration and electrical properties of Toro's surface.

a) Echo Bandwidth and Bounds on Radius

The edges of Toro's OC echo spectrum in Fig. 1 seem fairly well defined. The separation of "first zero crossings," interpolated from the two pairs of points straddling zero and closest to the echo center, is 14.4 Hz. The difference between this estimate for the edge-to-edge bandwidth (B) and the value (15.4 ± 0.9 Hz) derived from fitting the "$S(f)$" model to the data is clearly not too significant, but may nonetheless reflect bias in the latter caused by the symmetry inherent in the function $S(f)$. Accordingly, we adopt the average value, $B = 14.9 \pm 1.5$ Hz, as a "safe" estimate of the edge-to-edge bandwidth and its standard error.

What is the proper physical interpretation of B? Since Toro can be assumed to be a rigid body, the bandwidth at a given rotational phase is $B = (4\pi D/\lambda P)\cos\delta$, where P is Toro's synodic rotation period, δ is the Torocentric declination of the radar, and D is some effective diameter. In general terms, D is the sum of the distances, r_+ and r_-, measured from the plane containing the line of sight and Toro's rotation pole to those backscattering elements having the greatest positive (approaching) and negative (receding) line-of-sight velocities. For a sphere, $D = 2r_+ = 2r_-$ is the diameter. For a target that is nonspherical in the sense that $D(\Phi)$ is not constant, but still symmetrical in the sense that $r_+(\Phi) = r_-(\Phi)$, so the Doppler shift of the center of mass is halfway between the spectral edges, an estimate of bandwidth must be interpreted with care. If B is obtained from data with complete phase coverage, then D equals its maximum value, D_{max}. In the case of incomplete phase coverage, D is less than or equal to D_{max}, with equality holding only if the data sample at least one of the two (or more) rotational phases corresponding to the maximum bandwidth. We write: $D = \gamma D_{max}$, where $0 \leqslant \gamma \leqslant 1$ in general, and $\gamma = 1$ if phase coverage is complete. If phase coverage is not complete, the pattern of phase coverage can be used to derive an *a priori* probability distribution, $p(\gamma)$, for values of γ.

Toro is not necessarily symmetrical, but even if it were asymmetrical to the extent of having its center of mass on its surface, an estimate of bandwidth would still yield the following expression for the maximum distance (r_{max}) between the spin axis and a backscattering surface element: $r_{max} = B\lambda P/8\pi\gamma \cos\delta$. Our estimate ($B = 14.9 \pm 1.5$ Hz) of the bandwidth of the Fig. 1 spectrum yields: $r_{max}\gamma \cos\delta = 2.74 \pm 0.28$ km, and the phase coverage of our data is such that γ cannot be much less than unity [$p(\gamma > 0.94) = 1$ and $p(\gamma > 0.97) > 0.9$].

The principal source of uncertainty in Toro's r_{max} is due to uncertainty in Toro's pole direction, and hence in the Torocentric declination of Earth during our observations. DGH estimated Toro's pole direction using two very different methods. The first, called photometric astrometry (Taylor 1979), involves analysis of intervals between epochs of a certain light curve extremum. The second relies on comparison of the amplitudes of Toro light curves with the light curve amplitudes of laboratory models (Dunlap 1972). These methods gave pole directions (ecliptic longitude, latitude) equal to (150°, 45°) and (235°, 65°), respectively. DGH evaluated the relative merits of the two approaches and ultimately adopted the pole direction (200° ± 30°, 55° ± 7°).

If Toro's actual pole direction is (200°, 55°), then the subradar point stayed within 4° of Toro's equator throughout our 1980 July observations. Neither of the directions obtained by DGH's two methods places the subradar point as far as 20° from Toro's equator during any of our observations. Thus, despite the considerable uncertainty in Toro's pole direction, it seems unlikely that the 1980 July aspect was very far from equatorial. Assuming $\delta \leqslant 20°$, we obtain an interval estimate for the length of Toro's longest radius measured from the spin axis: $2.4 \text{ km} \leqslant r_{max} \leqslant 3.4$ km.

b) Radar Cross Sections and Circular Polarization Ratio

Integrating our weighted mean OC and SC spectra, we obtain the radar cross-section estimates: $\sigma_{OC} = 1.62 \pm 0.41$ km^2 and $\sigma_{SC} = 0.26 \pm 0.09$ km^2. Our quoted uncertainties are the root-sum-square of

*The term "standard error" denotes a standard deviation based solely on statistical errors in our data. In particular, we have *not* scaled quoted standard errors to make chi square per degree of freedom equal to unity.

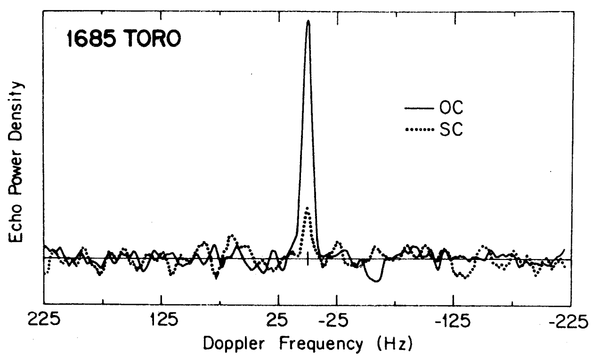

FIG. 2. Toro's average OC and SC echo power spectra, convolved with a model of the OC spectrum in Fig. 1 (see text). Echo power density is plotted on a linear scale.

standard errors (0.055 km^2 and 0.065 km^2, respectively) due to noise fluctuations and systematic errors (estimated to be 25% of the cross-section estimates) due to uncertainties in calibration of the radar system's sensitivity. Our value for σ_{OC} agrees reasonably well with the value, 1.3 km^2, reported by Goldstein *et al.* (1973).

The disparity between SC and OC contributions to Toro's radar echo is illustrated in Fig. 2, which shows weighted sums of the OC and SC echo power spectra. [To optimize signal-to-noise ratio (at the expense of frequency resolution) we smoothed the curves with a filter shaped like the "$S(f)$" model derived for the OC data in Fig. 1.] To obtain a representative value of Toro's circular polarization ratio, we formed a subset of OC data from those dates on which SC spectra were acquired, excluding OC runs that were (i) not overlapped by the sequence of SC runs on the same date and (ii) more than one run removed from a SC run. This precaution was motivated by the clear dependence of σ_{OC} on Toro's rotational phase. Our resultant weighted mean, $\mu_c = 0.18 \pm 0.04$, is derived from data spanning in three intervals (see below) a total of $\sim 200°$ of rotational phase. Appendix I outlines our calculation of errors associated with estimates of μ_c and other ratios reported herein.

The data used to estimate μ_c fall into three domains of rotational phase: 78°–187°, 237°–283°, and 330°–36°. Corresponding estimates of μ_c within these domains are 0.11 ± 0.07, 0.24 ± 0.06, and 0.19 ± 0.11, respectively. To the extent that the differences between these values are physically real, they represent heterogeneity in Toro's surface and/or subsurface structure at centimeter-to-meter scales. Further discussion of these polarization results is deferred until after we give a detailed description of Toro's OC spectral signature as a function of rotational phase.

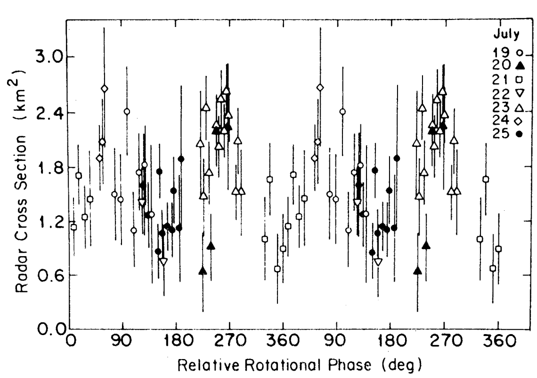

FIG. 3. Estimates of Toro's OC radar cross section, plotted against relative rotational phase (see text and Table I). The error bars represent plus and minus one-standard-deviation errors. Observation dates are encoded in the plotting symbols. Note from the abscissa scale that the data points have been plotted twice.

c) *Rotational Phase Dependence of Radar Cross Section*

Figure 3 plots all 47 measurements of Toro's OC radar cross section against rotational phase, encoding observation dates in the plotting symbols. Note that for certain domains of rotational phase, all available data were obtained on a single date. Since the azimuth/zenith-angle illumination trajectory of the Arecibo telescope depends on declination, and since Toro's declination changed by $\sim 12°$ during the course of our observations (Table I), we considered the possibility that systematic dependence of antenna gain on declination might have been responsible for the variations in σ_{OC} apparent in Fig. 3. We decided to reject this explanation because (i) we have calibrated, and corrected for, such gain variations using unpolarized, point radio sources whose flux densities at our feed frequency (2380 MHz) are well known; (ii) results of observations of several other Earth-crossing asteroids in 1980–1981 (Ostro *et al.* 1981, 1982) rule out the sort of declination dependence in antenna gain needed to explain the variations in Toro's radar cross section; and (iii) agreement between estimates of σ_{OC} for runs at similar Φ but on different dates is satisfactory.

With the 47 individual spectra ordered by rotational phase, we formed 47 "composite" spectra, each a weighted average of N consecutive individual spectra. With $N = 4$, we obtained an acceptable compromise between rotational phase resolution and signal-to-noise ratio. Radar cross sections derived from the four-run-composite spectra, plotted in Fig. 4(a), enhance the visibility of the extrema in Toro's "radar lightcurve." [Note that any two points in Fig. 4(a) are independent only if they have at least three points between them.]

The resemblance between the "radar lightcurve" in Fig. 4(a) and DGH's composite of optical light curves (reproduced here in Fig. 5) is striking, with σ_{OC} and V-filter brightness each showing an approximately two-fold variation. In each case, the light curve amplitude represents a weighted integration over the visible, illuminated portion of Toro's surface, where the weighting function is an appropriate scattering law. For optical

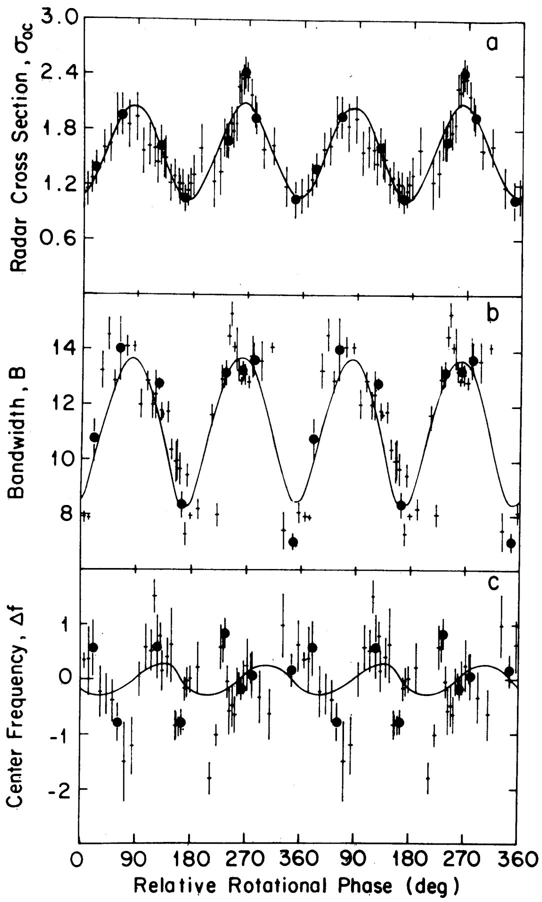

FIG. 4. Estimates of radar cross section (σ_{OC}, km^2), edge-to-edge bandwidth (B, Hz) and center frequency (Δf, Hz), derived from the four-run-composite spectra as described in the text and Appendix II. Note the "double plotting" as in Fig. 3. The vertical bars in (a) represent standard errors; those in (b) and (c) represent standard errors multiplied by root reduced chi square. The rotational phase of each point is a weighted mean of the phases corresponding to the four parent spectra, with the weighting factors determined from the noise in those spectra. Since each point is obtained from a four-run-average spectrum, any two points with fewer than three points between them are not independent. The eight independent spectra corresponding to the closed circles are plotted in Fig. 6. The curves, discussed in Sec. V, are based on spectra derived from the ellipsoid model described in Sec. IV.

light curves, the absence of rotational variations in either color or degree of polarization is considered evidence that an asteroid's light curve is due largely to its shape (Burns and Tedesco 1979). DGH surmised from their polarization measurements that Toro's light curve is dominated by shape, rather than reflectivity variations. On the basis of their laboratory model light curves, they concluded that Toro's light curve amplitude sets a lower limit, 1.9, on the ratio of maximum to minimum projected areas, and that ratios as large as 4.5 could not be excluded.

Although the prominent second-harmonic contribution to Toro's radar light curve suggests that the observed $\sigma_{OC}(\Phi)$ variation is largely determined by Toro's

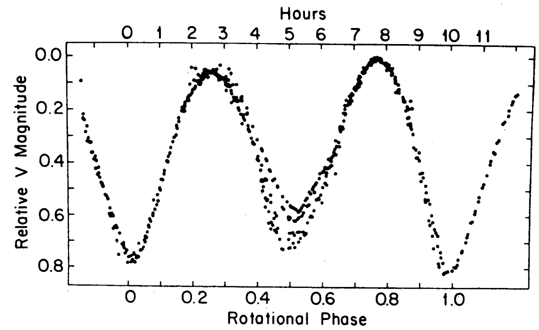

FIG. 5. Toro's optical light curve. This reproduction of Fig. 13 of Dunlap *et al.* (1973) shows these authors' composite of light curve data obtained in 1972 at solar phase angles from 32° to 76°. Relative V-filter magnitude is plotted against relative rotational phase. The central minimum is deepest at smallest phase angles, i.e., with illumination/viewing geometries closest to the radar backscattering configuration. The relation of zero rotational phase in this figure to that used elsewhere in this paper is unknown.

shape, the mixed effects of shape, reflectivity, and angular scattering law are not separable without recourse to some simplified model. Fortunately, Doppler resolution of the radar echoes provides additional leverage in determining Toro's shape.

d) Rotational Phase Dependence of Bandwidth

The closed circles in Fig. 4(a) correspond to a set of eight independent, four-run-composite spectra which adequately sample phases near the radar light curve extrema. These eight spectra, smoothed to 3-Hz resolution and plotted in Fig. 6, exhibit obvious variations in spec-

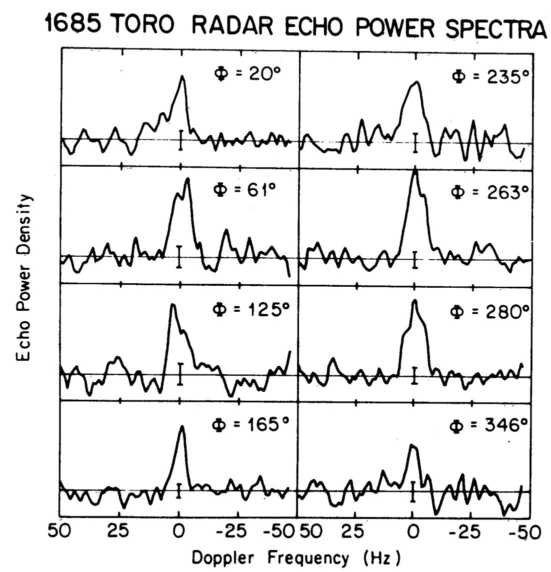

FIG. 6. The eight independent, four-run-composite spectra corresponding to closed circles in Fig. 4, here smoothed to a frequency resolution of 3 Hz. The error bars represent plus and minus one standard deviation of the background noise. The same linear scale is used for the ordinates in each section.

tral bandwidth. Unfortunately, the average signal-to-noise ratio of these spectra is inferior to that of the OC weighted mean spectrum in Fig. 1, so the spectral edges are comparatively ill defined, and the bandwidth (B) is more difficult to estimate precisely. Following the procedure outlined in Appendix II, we used a model of the form $S(f) \sim [1-(f-f_0)^2/(B/2)^2]^{n/2}$ to estimate B and f_0 for each of the 47 composite spectra used to generate Fig. 4(a). The results, plotted in Fig. 4(b), reveal an approximately twofold variation in B, in phase with the radar light curve. Note that the bandwidth estimates reach maxima of similar magnitude, whereas the radar and optical light curves have distinct primary and secondary maxima. This difference is quite reasonable, since the "true" bandwidth curve for a rotating radar target observed at constant astrocentric declination would have no odd-harmonic Fourier components.

Figure 4(c) plots estimates of $\Delta f = f_0 + 2.8$ Hz vs rotational phase for the four-run composite spectra. These values of Δf have a mean within 0.1 Hz of zero and a rms fluctuation equal to ~ 0.7 Hz (or $\sim 5\%$ of the maximum spectral bandwidth). Inspection of the spectra indicates that the variations in Δf reflect primarily variations in spectral shape, rather than variations in spectral position. Evidence for a strong first-harmonic wobble in center frequency, such as that found for 433 Eros (Jurgens and Goldstein 1976), is not apparent in Fig. 4(c), suggesting that Toro may be more symmetrical (in the sense defined earlier) than Eros.

IV. MODELS OF TORO'S SHAPE

The variations in Toro's echo characteristics (i.e., cross section, polarization ratio, spectral bandwidth, and center frequency) suggest a nonspherical shape or an inhomogeneous scattering law, or both. In this section we explore representations of Toro's radar signature by models postulating an idealized asteroidal shape, viz., either a triaxial ellipsoid or a cylinder with hemispherical ends. In each case we compute model echo spectra based on a homogeneous radar backscattering law, $\sigma_0(\theta) = R \cos^n \theta$, where R is an amplitude scaling factor whose physical interpretation will be addressed below.

The utility of a triaxial ellipsoid model for interpretation of radar signatures of nonspherical targets was demonstrated by Jurgens and Goldstein (1976) in their analysis of λ 3.5-cm echoes from 433 Eros. Capitalizing on their experience, we have applied a similar approach to the Toro data and have adopted the technique developed by Jurgens (1982) for calculating echo spectra.

In its most general form, an ellipsoid model would contain at least the ten free parameters: n; R; the semiaxis lengths $a \geqslant b \geqslant c$, where rotation is about the c axis; the magnitude and two directional coordinates of the spin vector; the rotational phase Φ_0 at a suitably defined epoch; and the frequency f_0 corresponding to the Doppler shift of echoes from the model's center of mass. Since the number of available degrees of freedom in an estimation problem equals the number of data points less the number of free parameters, fitting a single ten-parameter model to the entire set of 47 OC spectra largely eliminates convergence problems encountered when using an iterative, linearized procedure to fit a three- or four-parameter model independently to each spectrum.

As discussed at length by Jurgens (1982) and Jurgens and Goldstein (1976), the high correlation between estimates of certain parameters often precludes their accurate joint estimation. For instance, our data cannot provide clean separation of R and c, whose linear correlation coefficient is between -0.99 and -1.00. Furthermore, exploratory calculations showed that our data are insufficiently sensitive to the components of Toro's spin vector to warrant an attempt to obtain independent estimates of those parameters. This lack of sensitivity is due to (i) the limited signal-to-noise ratio in our data, (ii) *a priori* uncertainty in Toro's size and shape, and (iii) Toro's nearly equatorial aspect, for which echo bandwidth is a very slowly changing function of the Torocentric declination of the radar (δ). We therefore assumed an equatorial aspect ($\delta = 0°$) and a constant synodic period equal to 10.176 hr. Setting $b = c$ leaves a vector of six free parameters, $\mathbf{x} = (a,b,n,R,\Phi_0,f_0)$, with Φ_0 the rotational phase (modulo 180°) minimizing the angle between the line of sight and the a axis. Analyses discussed above provided a reliable initial guess for the region of parameter space likely to contain the weighted-least-squares estimate for $\mathbf{x}$.

Direct searches in parameter space over increasingly fine grids combined with an iterative, linearized technique located the point ($\hat{\mathbf{x}}$) at which chi square reaches a global minimum. Table II gives our weighted-least-squares parameter estimates, their standard errors, and the correlation matrix corresponding to our ellipsoid

TABLE II. Ellipsoid model.

Parameter	Estimate	Correlation matrix a	b	n	R	Φ_0	f_0
a(km)	2.60 ± 0.10	1					
$b = c$(km)	1.68 ± 0.17	0.73	1				
n	2.04 ± 0.45	0.73	0.87	1			
R	0.22 ± 0.02	-0.02	-0.19	0.28	1		
Φ_0	$172° \pm 4°$	-0.01	-0.07	-0.02	0.08	1	
f_0(Hz)	-2.8 ± 0.1	-0.04	-0.02	0.00	0.03	0.11	1

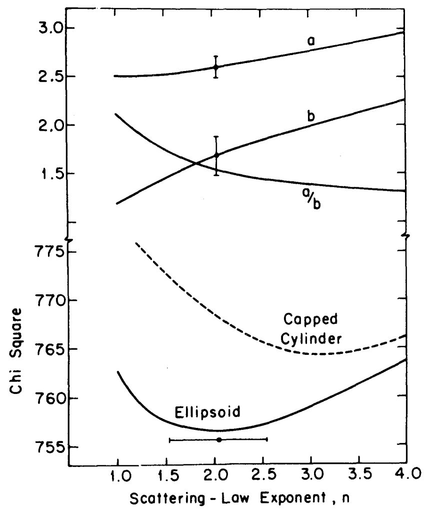

FIG. 7. Values of the equatorial semiaxis lengths a and b (in kilometers) and their ratio, estimated from an ellipsoid model for different values of the scattering-law exponent n, with other parameters fixed at their values in Table II. The closed circles and error bars show estimates and standard deviations for a, b, and n derived from the six-parameter estimation. Note that the correlation of b with n is more severe than the correlation of a with n, and that the correlation of a with b increases with n. Values of the chi square statistic, calculated on the basis of 605 degrees of freedom, is shown for the ellipsoid and capped-cylinder models.

model. Figure 7 illustrates the statistical relations between estimates of a, b, and n. Within the standard errors, the value for f_0 agrees with that derived in Sec. III, and the estimate of Φ_0 agrees with that calculated from an even-harmonic Fourier series derived for the 47 samples of σ_{OC} plotted in Fig. 3.

Figure 7 also compares the behavior of chi square vs n for the ellipsoid model to that for the capped cylinder model. The cylinder model gave values of a (half the distance between the ends of the caps) systematically about 0.1 km smaller than corresponding values derived from the ellipsoid model, whereas values for b (the cylinder radius) generally differed by about 0.05 km. The cylinder model yields a higher value of n (corresponding to more limb darkening) than does the ellipsoid model. Since the chi square curves in Fig. 7 suggest that the cylinder model is inferior (or at least not superior) to the ellipsoid model, the cylinder model will not be discussed further.

As an internal check on our ellipsoid model, we used it to generate a 47-run, weighted-mean spectrum and then fit to this spectrum the same function, $S(f) = [1 - (f - f_0)^2/(B/2)^2]^{n/2}$, used in Sec. II to analyze Toro's weighted-mean echo power spectrum (Fig. 1). The values ($B = 14.9 \pm 0.9$ Hz and $n = 3.6 \pm 1.4$) for the bandwidth and "shape factor" estimated from the ellipsoid-model spectrum agree with those ($B = 15.4 \pm 0.9$ Hz, $n = 3.6 \pm 1.4$) estimated from the data.

We examined the sensitivity of our data to the Torocentric declination of the radar by fixing f_0 and Φ_0 to their Table II values and estimating a, b, n, and R for fixed, nonzero values of δ. For $\delta = 10°$ and $\delta = 20°$, we obtain chi square minima (756.635 and 757.555) higher than the value (756.533) for $\delta = 0°$, a result which supports (or at least fails to contradict) the inference that Toro's aspect was nearly equatorial during our observations. Estimates of a increase roughly as $1/\cos\delta$, from 2.60 ± 0.10 km with $\delta = 0°$ to 2.65 ± 0.10 with $\delta = 10°$ and 2.78 ± 0.10 with $\delta = 20°$. Changes in b, n, and R are much less significant, resulting in values well within the quoted uncertainties in the Table II values.

As noted above, the high correlation between c and R prevents us from obtaining meaningful independent estimates of these parameters. Nevertheless, it is interesting that estimations of a, b, n, and R employing fixed values of c show that best-fit values of chi square decrease relative to the Table II value (756.533) as c decreases, reaching a minimum of 756.529 near $c = 1.28$ km. Unfortunately, treating both c and R as free parameters makes standard errors in these parameter estimates larger than the estimates themselves. In any case, since the model ellipsoid rotates about its c axis, our Table II estimate of b provides an upper limit on physically acceptable values for c (barring a "recent" collision). Consequently, our estimated value of the amplitude scaling factor, $R = 0.22 \pm 0.02$, should be considered a lower limit.

As noted by Jurgens and Goldstein (1976), physical interpretation of R requires knowledge of the actual bistatic scattering law, $\sigma_0(\theta_i, \theta_r)$, where the arguments are angles of incidence and reflection. Let us assume an azimuthally isotropic law of the form $\sigma_0(\theta_i, \theta_r) = \rho g \cos\theta_i (\cos\theta_r)^{n-1}$, where ρ is the Fresnel power reflection coefficient at normal incidence ($\theta_i = \theta_r = 0$), g is a constant gain factor, and $n \geqslant 0$. Then conservation of energy requires that $g = 2n$, so $R = 2n\rho$ in our ellipsoid model, and the estimate, $\rho = 0.054^{+0.014}_{-0.010}$ follows from the parameter estimates in Table II and the error analysis in Appendix I.

We will return to a discussion of Toro's radar scattering properties below, but let us pursue interpretation of our estimate of ρ within the framework of the ellipsoid model and our stated assumptions. Suppose our best-fit ellipsoid is composed of L-chondritic material of advanced petrologic type, as suggested by the reflection spectroscopy of Chapman *et al.* (1973). Campbell and Ulrichs (1969) measured the electrical properties of three L6 chondrites (Bruderheim, Colby, Holbrook) at microwave frequencies straddling our own. For solid samples, they determined values for the real part ϵ of the dielectric constant which satisfy $7.8 \leqslant \epsilon \leqslant 11.8$. (Values for the loss tangent are less than 0.06 and are negligible for our purposes.) Powdered samples showed very good agreement with predictions of the Rayleigh mixing law, which relates the porosity (i.e., the fraction of the volume that is empty) to the dielectric constants of solid and powdered forms of a material. For a lossless dielectric, $\rho = 0.054$ corresponds to $\epsilon = 2.55$, which would characterize L6 chondritic powder with a porosity within several percent of 54%.

This line of reasoning has assumed that Toro's OC echo results from single reflection from a homogeneous, smooth, dielectric interface. However, Toro's nonzero circular polarization ratio ($\mu_c = 0.18 \pm 0.04$) suggests the possibility that multiple scattering contributes to the OC echo. Suppose we model the echo as the (incoherent) sum of (i) a polarized component (with $\mu_c = 0$) due to single reflections from smooth facets, and (ii) a multiply scattered component (with $\mu_c = 1$). Then, following the approach of Ostro *et al.* (1980), we calculate that only 69% of the total OC echo power would be due to the first of these components, reducing our estimates for R and ρ accordingly. Considering this possibility, as well as the formal uncertainty in estimation of ρ and the variations in ϵ among L6 chondrites, we calculate porosities which fall within the range spanned by $56\% \pm 12\%$, assuming $c = b$. Of course, models with $c < b$ would have smaller porosities. For comparison, the porosity of the top 5 to 10 cm of lunar soil is typically between 30% and 60% (Carrier *et al.* 1973).

V. DISCUSSION

How good a fit to the data is provided by the ellipsoid model? In order to optimize the sensitivity of chi square to departures of the data from the model, we calculate this statistic using only the 13 points closest to the center of the echo in each spectrum. For a six-parameter fit, the 47 spectra provide 605 degrees of freedom, and the probability that the Gaussian noise in the data accounts for chi square as large as the minimum values obtained for our ellipsoid model is less than 0.0001. In other words, the post-fit residuals are too large to be due to noise alone and must be explained instead by systematic differences between Toro and our ellipsoid model.

a) Departures from the Ellipsoid Model

The curves in Fig. 4 were generated from four-run-composite spectra derived from the ellipsoid model. Differences between the points and curves for the functions $\sigma_{OC}(\Phi)$, $B(\Phi)$, and $\Delta f(\Phi)$ exist because Toro has a non-ellipsoidal shape and/or an inhomogeneous scattering law (with n and/or R varying over the surface). The relative importance of these factors is difficult to ascertain.

Examination of the post-fit residuals as a function of frequency and rotational phase reveals only a single candidate for a radar "feature," namely a set of spectrally centered positive residuals near $\Phi \approx 260°$, on the maximum of the radar light curve. Recalling our estimates of the circular polarization ratio within three domains of rotational phase, we note that the largest estimate for μ_c falls in the region $237° \leqslant \Phi \leqslant 283°$. This result, coupled with the relatively good agreement between the model and the data for estimates of bandwidth [Fig. 4(b)] and center frequency [Fig. 4(c)] near these phases, suggests that the residuals near $\Phi \approx 260°$ are probably caused by a localized region of enhanced surface roughness and backscattering efficiency, rather than by departures of Toro's gross shape from an ellipsoid.

b) Axis Ratio

As illustrated in Fig. 4(b), the ratio of maximum to minimum bandwidth estimated for the data exceeds that estimated for the ellipsoid model, possibly due to the model's intrinsic symmetry. It appears likely that the actual ratio of Toro's maximum to minimum equatorial widths exceeds our model's axis ratio, $a/b = 1.55^{+0.13}_{-0.11}$. (If the Torocentric declination of the radar is forced to equal 20°, the ratio increases by $\sim 6\%$.) However, visual inspection of the points in Fig. 4(b) suggests that it might be difficult to reconcile these data with an axis ratio very much larger than about 2.2.

Jurgens and Goldstein (1976; see also Jurgens 1982, p. 106) point out that for an actual ellipsoid with a $\cos^2\theta$ scattering law, the axis ratio is overestimated by the ratio of maximum-to-minimum values of either the bandwidth or the radar cross section. They note that the bias is much more severe for the cross-section ratio than for the bandwidth ratio, but do not give quantitative estimates for the biases. For our model, with $a/b = 1.55$, the bandwidth ratio is 1.6 and the cross-section ratio is 2.1. Considering all factors, we arrive at approximate bounds for the ratio of Toro's longest to shortest equatorial axes: $1.4 < a/b < 2.2$

If Toro were a triaxial ellipsoid, a/b would equal the ratio, A_{max}/A_{min}, of extreme values for Toro's projected area (as seen by a distant observer at a Torocentric declination, $\delta = 0°$). Since Toro's shape and pole direction are not well known, the precise relation between a/b and A_{max}/A_{min} cannot be specified. Nevertheless, our radar-derived bounds on a/b suggest that Toro's A_{max}/A_{min} might be less than the value (3.2 ± 0.7) deduced by DGH from their photopolarimetry. Discussing their method for estimating A_{max}/A_{min}, DGH note that given the primary amplitude of Toro's optical light curve (~ 0.75 mag), "none of the available [laboratory model lightcurve] data permit the ratio to be less than 1.9, assuming that Toro does not have large reflectivity variations over the surface...." Of course, if Toro's geometric albedoes at the optical light curve maxima were systematically higher than those at light curve minima, the light curve amplitude would overestimate the projected area ratio, A_{max}/A_{min}.

c) Size and Optical Geometric Albedo

DGH estimated Toro's size from their photopolarimetry at solar phase angles between 32° and 99°, as follows. By fitting straight lines to measurements of (i) absolute V-filter magnitude at times of primary light curve maxima, (ii) $B - V$ color, and (iii) B-filter percentage of polarization as functions of solar phase angle, they derived values for Toro's maximum B-filter magnitude

[$B(1,0) = 14.62$ mag], and the slope of the polarization vs phase curve ($h = 0.13$ percent deg^{-1}). From the empirical slope-albedo law and the definition of geometric albedo (Bowell and Zellner 1973), DGH derived a B-filter geometric albedo, $p_B = 0.14 \pm 0.03$, and an equivalent radius, $r \equiv (A_{\max}/\pi)^{1/2} = 2.8 \pm 0.6$ km for Toro at primary light curve maximum.

We convert DGH's result to an estimate of Toro's maximum cross-sectional area, $A_{\max} = \pi r^2 = 24.6 \pm 10.5$ km^2, for comparison to the value derived from our ellipsoid model, $A_{\max} = \pi ac \leqslant 13.7 \pm 1.8$ km^2. (If the Torocentric declination of the radar is set equal to 20°, this estimate increases to 14.8 ± 1.8 km^2.) To the extent that our ellipsoid model constitutes an accurate estimator of $A_{\max}$, our calculations suggest a value no more than 60% as large as that deduced by DGH, but within one standard error of their value.

This constraint on $A_{\max}$, when combined with DGH's color and absolute magnitude measurements, provides limits on Toro's B and V geometric albedoes: $p_B \geqslant 0.23$, $p_V \geqslant 0.28$. A comment by Chapman *et al.* (1973) lends some confidence to the validity of our results: "Meteorites having absorption bands as deep as Toro's have geometric albedoes in excess of 20% and more commonly 30%. Hence, there is at least a suggestion that Toro may be somewhat brighter, and hence smaller, than Dunlap *et al.* (1973) conclude from the slope of the polarization-versus-phase curve."

d) Radar Scattering Properties and Surface Structure

An estimate of radar cross section (e.g., σ_{OC}) becomes a useful measure of radar reflectivity when normalized to the target's projected area. Our ellipsoid model (Table II) yields a limit on Toro's *normalized* OC radar cross section, $\hat{\sigma}_{OC} \geqslant 0.14 \pm 0.04$. Using our estimate for Toro's average circular polarization ratio, we derive a limit on Toro's λ 13-cm geometric albedo, $p_{13\text{cm}} \equiv (1 + \mu_c)\hat{\sigma}_{OC}/4 \geqslant 0.04 \pm 0.01$.

Toro's λ 13-cm $\hat{\sigma}_{OC}$ exceeds corresponding mean values estimated for the Moon, Mercury, Venus, and Mars (see Pettengill 1978 for references). However, the value of this comparison is limited because the radar signatures of these terrestrial planets are, for the most part, very different from Toro's. Their sharply peaked spectra, due to a quasi-specular scattering process, indicate surface regions that are extremely smooth at scales from a few centimeters to at least a meter, with rms slopes $\lesssim 10°$ at 10-to-100-m scales. In contrast, the total absence of sharply peaked spectra in the Toro data requires considerable roughness at some scale(s) at least as large as several centimeters.

The ratio μ_c is a convenient indicator of the roughness of a planetary surface at scales within about an order of magnitude of the observing wavelength. A value of μ_c near zero would require that the echo be due almost entirely to single reflections from smooth surface elements. At the opposite extreme, μ_c would approach unity for complete depolarization of the incident wave because of extreme small-scale roughness or multiple scattering. For Toro, μ_c is larger than the λ 13-cm values [0.04 (Goldstein 1970), 0.05 (Levy and Schuster 1964), 0.06 (Carpenter 1966)] reported for Venus, and the λ 23-cm value (0.1) reported by Evans and Hagfors (1966) for the Moon, but lower than the λ 13-cm average value (0.37) recently obtained by Harmon *et al.* (1982) for parts of Mars. Whereas Toro's radar echo appears dominated by single reflection from smooth surface elements, the magnitude of Toro's μ_c requires a modicum of surface and/or subsurface roughness at centimeter-to-meter scales. However, since $\mu_c \ll 1$, this small-scale roughness seems insufficient to account for Toro's very nonspecular spectral signature. In other words, considerable roughness is required at ~10 to ~100 m scales. These are presumably the structural scales responsible for the nearly Lambertian ($n = 2$) limb darkening of our ellipsoid model.

VI. CONCLUSION

Using the results of the 1980 radar observations and the 1972 VIS/IR observations, we offer the following description of Toro as a working hypothesis: "Toro's shape is elongated and irregular, with extreme projected areas in the ratio ~1.6, and extreme equatorial widths in the ratio ~1.9. For an equatorial view, Toro's mean effective diameter [i.e., $(4A_{\text{proj}}/\pi)^{1/2}$, with A_{proj} the mean projected area] is ~3.3 km. Toro's regolith has a porosity comparable to that of lunar soil, and a slightly higher areal concentration of centimeter-to-meter-sized blocks within a few meters of the surface. The surface is much rougher than the Moon at 10-to-100 meter scales, and is marked by variations in optical albedo and decimeter-scale roughness." (Of course, the uncertainties associated with our derived constraints on Toro's physical properties permit substantial deviation from the "nominal" values incorporated into this description.)

Toro should be observed radiometrically and photopolarimetrically during its February 1984 apparition to elucidate the source of the discrepancy between polarimetric and radar size estimates, and to refine existing knowledge of the spin vector.

Although Toro remains beyond Arecibo's maximum-sensitivity window until 1988, more than a dozen other Earth-approaching asteroids (including 1627, 2101, 2340, 1982BB, and 1982RA) can be scrutinized with λ 13-cm radar in the interim. As others have noted, and as this paper demonstrates, the investigative power of several astronomical techniques applied in parallel to a given target greatly exceeds that of any one technique used in isolation.

We are indebted to R. Jurgens for providing his algorithm for generating ellipsoid-model spectra well in advance of its publication. We thank B. Marsden for providing information useful in preparation of the ephemerides; A. Forni for calculation of the ephemerides; R. Velez, T. Dickinson, and the staff of the Arecibo

Observatory for assistance with the observations; B. McFarlane and K. Vogel for programming assistance; M. Roth and J. Riley for secretarial assistance; B. Boettcher for drafting the figures; and L. Dunlap, J. Gradie, S. Schwager, and J. Veverka for valuable discussions. This research was supported in part by NASA Grant NAGW-116 (Ostro) and in part by NSF Grant PHY78-07769 (Shaprio). The Arecibo Observatory is part of the National Astronomy and Ionosphere Center.

APPENDIX I: ERRORS IN ESTIMATES OF RATIOS

Suppose that x_1, x_2 are unbiased estimates of X_1, X_2, obtained as linear functions of observations contaminated by normally distributed errors with variances v_{11} and v_{22} and covariance v_{12}. Defining $m = x_1/x_2$ as an estimate of $\mu = X_1/X_2$, Fieller's theorem (Finney 1964) sets upper and lower limits on μ:

$$m_U = [m - gv_{12}/v_{22} + Y]/(1-g),$$
$$m_L = [m - gv_{12}/v_{22} - Y]/(1-g),$$

where

$$Y = (t/x_2) \times [v_{11} - 2mv_{12} + m^2v_{22} - g(v_{11} - v_{12}^2/v_{22})]^{1/2},$$
$$g = t^2 v_{22}/x_2^2,$$

and t is Student's t statistic with ν degrees of freedom at a specified significance level. For our purpose, ν is so large that the distribution of t is nearly normal. By setting $t = 1$, we determine limits with the same probabilistic connotation as values one standard deviation from a parameter estimate. In other words, the probability that $m_L \leqslant \mu \leqslant m_U$ is 0.68. If $m = (m_L + m_U)/2$, we express the ratio estimate as $m \pm (m_U - m_L)/2$.

APPENDIX II: FITS TO COMPOSITE SPECTRA

Acknowledging the high correlation between least-squares estimates of B and n for a model of the form $S(f) \sim [1 - (f - f_0)^2/(B/2)^2]^{n/2}$, we fit such a model to each of the 47 four-run-composite spectra used to generate Fig. 4(a), but with fixed n. Repeating this procedure for various values of n between 0.6 and 3.0, we found that estimated values of B increased systematically with n. However, all these fits reveal a consistent pattern, namely an approximately twofold variation in B, in phase with the radar light curve. The weighted sum of squared residuals (i.e., chi square) as a function of n shows a broad minimum, centered near $n = 1.4$.

Although fixing the shape parameter n necessarily introduces some bias in estimates of B, our iterative linearized procedure for simultaneous estimation of n and B often encounters serious convergence problems when applied to the four-run composite spectra. A convenient compromise solution is to substitute a less severe constraint for the "hard," fixed-n constraint. Accordingly, we plot in Fig. 4(b) values of $B(\Phi)$ for the composite spectra, estimated under the prior constraint (Bard 1974): $n = 1.4 \pm 0.5$. This "radar bandwidth curve" is likely a more accurate representation of the data than any based on a fixed value of n, but the general pattern is representative of fixed-n fits.

In estimating B for the four-run-composite spectra, we fixed the center frequency at the value (-2.8 Hz) estimated earlier from the weighted mean OC spectrum. For asymmetrical spectra, this constraint can exert a positive bias on estimates of B. Repeating the procedure used to generate the points in Fig. 4(b), but treating f_0 as a free parameter, we obtain values of B systematically ~ 1 Hz lower than those in Fig. 4(b), but again leaving the pattern of $B(\Phi)$ variation unchanged. Figure 4(c) plots our estimates of $\Delta f = f_0 + 2.8$ Hz.

REFERENCES

Bard, Y. (1974). *Nonlinear Parameter Estimation* (Academic, New York), p. 32.

Bowell, E., and Zellner, B. (1973). In *Planets, Stars and Nebulae Studied with Photopolarimetry*, edited by T. Gehrels (University of Arizona Press, Tucson), p. 381.

Burns, J. A., and Tedesco, E. F. (1979). In *Asteroids*, edited by T. Gehrels (University of Arizona Press, Tucson), p. 494.

Campbell, D. B., Pettengill, G. H., and Shapiro, I. I. (1976). Icarus **28**, 17.

Campbell, M. J., and Ulrichs, J. (1969). J. Geophys. Res. **74**, 5867.

Carpenter, R. L. (1966). Astron. J. **71**, 142.

Carrier, W. D. III, Mitchell, J. K., and Mahmood, A. (1973). *Proceedings of the Fourth Lunar Science Conference* (Pergamon, New York), p. 2403.

Chapman, C. R., and Zellner, B. H. (1978). In *Asteroids: An Exploration Assessment*, edited by D. Morrison and W. C. Wells (NASA Conference Publication 2053), p. 183.

Chapman, C. R., McCord, T. B., and Pieters, C. (1973). Astron. J. **78**, 502.

Dunlap, J. L., Gehrels, T., and Howes, M. L. (1973). Astron. J. **78**, 491 (DGH).

Dunlap, J. L. (1972). *Laboratory Work on the Shape of Asteroids*, M.S. thesis (University of Arizona, Tucson).

Finney, D. J. (1964). *Statistical Method in Biological Assay*, 2nd ed. (Hafner, New York), p. 24.

Goldstein, R. M., Holdridge, D. B., and Lieske, J. H. (1973). Astron. J. **78**, 508.

Goldstein, R. M. (1970). Radio Sci. **5**, 391.

Goldstein, R. M. (1969). Icarus **10**, 430.

Goldstein, R. M. (1968). Science **162**, 903.

Greenberg, R., and Scholl, H. (1979). In *Asteroids*, edited by T. Gehrels (University of Arizona Press, Tucson), p. 310.

Harmon, J. K., Campbell, D. B., and Ostro, S. J. (1982). Icarus **52**, 171.

Johnson, T. V., and Matson, D. L. (1973). Astron. J. **78**, 505.

Jurgens, R. F. (1982). Icarus **49**, 97.

Jurgens, R. F., and Bender, D. F. (1977). Icarus **31**, 483.

Jurgens, R. F., and Goldstein, R. M. (1976). Icarus **28**, 1.

Levy, G. S., and Schuster, D. (1964). Astron. J. **69**, 29.

Morrison, D., and Niehoff, J. (1979). In *Asteroids*, edited by T. Gehrels (University of Arizona Press, Tucson), p. 227.
Ostro, S. J., Campbell, D. B., and Shapiro, I. I. (1981). Bull. Am. Astron. Soc. **13**, 716.
Ostro, S. J., Campbell, D. B., Shapiro, I. I., and Showalter, M. R. (1982). Bull. Am. Astron. Soc. **14**, 725.
Ostro, S. J., Campbell, D. B., Pettengill, G. H., and Shapiro, I. I. (1980). Icarus **44**, 431.
Pettengill, G. H. (1978). Annu. Rev. Astron. Astrophys. **16**, 265.
Pettengill, G. H., and Jurgens, R. F. (1979). In *Asteroids*, edited by T. Gehrels (University of Arizona Press, Tucson), p. 206.
Pettengill, G. H., Shapiro, I. I., Ash, M. E., Ingalls, R. P., Rainville, L. P., Smith, W. B., and Stone, M. L. (1969). Icarus **10**, 432.
Snedecor, G. W., and Cochran, W. G. (1980). *Statistical Methods*, 7th ed. (Iowa State University Press, Ames).
Taylor, R. C. (1979). In *Asteroids*, edited by T. Gehrels (University of Arizona Press, Tucson), p. 480.
Williams, J. G., and Wetherill, G. W. (1973). Astron. J. **78**, 510.